J Appl Electrochem (2009) 39:513–521
DOI 10.1007/s10800-008-9708-y

ORIGINAL PAPER

# Morphology and electrochemical activity of SOFC composite cathodes: I. experimental analysis

**Antonio Barbucci · M. Paola Carpanese · Massimo Viviani · Nicolaos Vatistas · Cristiano Nicolella**

Received: 3 September 2008 / Accepted: 24 October 2009 / Published online: 14 November 2008


**Abstract** This paper describes the first part of an experimental and theoretical study performed on composite Lanthanum Strontium Manganite (LSM) and Yttria-stabilized Zirconia (YSZ) electrodes. Cathode electrocatalytic activity was investigated using different cell configurations and carrying out potentiodynamic polarisation and electrochemical impedance spectroscopy measurements (EIS). Measurements were carried out at different oxygen partial pressures, overpotentials, temperatures and electrode geometries. In order to identify the main steps involved in cathodic oxygen reduction, the NLLS-Fit procedure was used. The results for different cell geometries agree with each other, suggesting a transition in the overall reaction mechanism, from charge transfer to mass transfer control, at a critical temperature of about 750 °C. The experimental results also show a remarkable effect of electrode thickness on the overall reaction rate, throughout the temperature range tested. A grey level gradient along the thickness of the thicker electrodes were detected by analyzing microscopic images of the cells. These results, together with electrochemical measurements on cathodes with different thickness, confirm that morphology plays a key role in determining the performance of Solid Oxide Fuel Cells (SOFC) composite cathodes.

**Keywords** Active sites · LSM/YSZ composite electrode · Modelling · Electrochemical measurements · Solid oxide fuel cells

A. Barbucci (✉) · M. Paola Carpanese
Department of Chemical and Process Engineering, University of Genoa, P.le J.F. Kennedy 1, 16129 Genoa, Italy
e-mail: barbucci@unige.it

A. Barbucci · M. Paola Carpanese · M. Viviani
Interuniversity Consortium on Materials Science and Technology, Via G. Giusti 9, 50121 Florence, Italy

M. Viviani
Institute for Energetics and Interphases, Via E. De Marini 6, 16149 Genoa, Italy

N. Vatistas · C. Nicolella
Department of Chemical Engineering, Industrial Chemistry and Materials Science, Via Diotisalvi 2, 56126 Pisa, Italy

## 1 Introduction

Electrodes for Solid Oxide Fuel Cells (SOFCs) are designed to maximise the active area for electrochemical processes. Mixed ionic and electronic conductors (LSC [1], LSCF [2], BSCF [3] for the cathode; Fe-doped Ceria [4], LSCM [5] for the anode) as well as mixtures of electronic conductors electrocatalyst and ionic conductor electrolyte materials have been widely used and studied for this purpose [6]. Practice has shown that, in order to achieve effective and long lasting cell performance, other aspects need to be carefully taken into account, in addition to the active area. Typically, to obtain a good current distribution at the interconnect/electrode interface, a porous layer containing electrocatalyst material is deposited and works as current collector/distributor [7]. On the same side, in order to prevent electrode poisoning by elements normally contained in the interconnects (for instance Cr), a very thin compact layer with possibly high electronic conductivity is grown on the interconnect surface [8]. This layer also acts to prevent metallic interconnect oxidation. Recently, an additional thin functional layer has been included in the electrode/electrolyte interface [9, 10] to improve electrode electrochemical activity. This is often similar to the bulk electrode, but with a different grain size distribution and

morphology. Moreover, impregnation of macroporous electrodes with nanoparticles has been investigated, to enhance electrochemical activity or catalytic activity, if direct hydrocarbon oxidation is performed at the fuel electrode. With this multiphase porous microstructure, composite electrodes can give different performances depending on porosity, specific surface area ($m^2\ m^{-3}$) available for the electrochemical reaction, as well as ionic and electronic conductivities of the different phases. More detailed information is required about the main factors governing oxygen reduction kinetics, in order to inform electrode design and improve cell performance.

One of the crucial issues is the real distribution of active sites within the electrode, if a random composite structure is considered [11, 12].

In this paper, the cathodic side of the cell, which is a main source of irreversibility in hydrogen fed SOFCs, has been investigated, having regard to all these aspects. Materials with very low mixed conductivity have been considered, in order to ensure that charge transfer processes are mainly localised at the Three Phase Boundary points (TPB). In particular, the cathode is composed of a Lanthanum Strontium Manganite (LSM) and Yttria-stabilized Zirconia (YSZ) mixture, the most conventional and stable couple of materials for application in SOFCs, due to their chemical stability and compatibility [13–15]. New experimental results are presented which extend previously published data [16]. These data form a sound basis for the theoretical analysis of charge transport and electrochemical reaction in the cathode, as presented in a companion paper [17].

## 2 Experimental

Electrolyte supported cells in typical symmetrical two-electrode and three-electrode configurations were used. The electrolyte pellet was made by pressing 2.5 g of 8 mol% $Y_2O_3$ + 92 mol% $ZrO_2$ powders (TZ-8YS Tosoh powder with 0.3 μm particles assembled in 40 μm agglomerates) at 5 tons and sintering at 1,500 °C for 5 h. The final result was a 20 mm diameter and about 2 mm thick ceramic disk. This thickness was chosen to avoid measurement errors due to misalignment of working and counter electrodes [18, 19]. The cathodes were prepared by overnight wet ball-milling of equal volumes of YSZ and $(La_{1-x}Sr_x)_y\ MnO_{3\pm\delta}$ ($x = 0.25$ and $y = 0.95$; Praxair, about 0.3 μm). The mixture was then dried and diluted in α-Terpineol (Aldrich). Further milling was performed to obtain a paste that could easily be applied to the YSZ pellet surface by slurry coating. The electrode was then fired at 1,100 °C for 1 h (heating range 5 °C/min). From a geometrical point of view, the LSM/YSZ electrodes were arranged on the circular surfaces of the solid electrolyte, in order to achieve experimental conditions based on cylindrical symmetry. Different LSM/YSZ cathodes were prepared with different thickness ranging between 5 and 120 μm. In order to reach equi-potential conditions (i.e. homogeneous distribution of current lines), a thin current collector layer, made up of coarse LSM powder mixed with Terpineol, was applied to the working electrode surface in contact with the external circuit wires. A Pt counter-electrode, with the same shape and position as the working electrode, was painted on the opposite side of the electrolyte pellet. For two-electrode measurements, symmetrical cells were prepared by depositing LSM/YSZ counter-electrodes. The Pt-reference and counter electrodes were fired at 900 °C for 1 h. In the three-electrode configuration, a Pt reference (Pt ink 6926 Engelhard, particle size 12 μm) electrode was painted around the working or the counter electrode, and care was taken to leave as large a distance as possible between the two electrodes, in order to prevent systematic errors in electrochemical measurements.

The cells were placed in a rig inside an alumina shoe sliding over an alumina supporting tube [20], inserted in a tubular furnace. Measurements were carried out between 500 and 900 °C, at different polarisations and varying oxygen partial pressures. The temperature was checked by a thermocouple placed close to the cell (1 cm).

The cell was connected to the electrochemical instruments through platinum wires, which were shielded to reduce noise. EIS and potentiodynamic measurements were conducted for electrochemical investigations. EIS analyses were performed using a 1286 Solartron electrochemical interface and a 1260 Solartron Frequency Response Analyzer, over a 0.1 Hz–100 kHz frequency range, with 20 mV A.C. signal amplitude, at equilibrium potential and under polarisation conditions. The cell was left at the highest temperature for 24 h before starting the measurements.

After electrochemical investigation, the cells were analysed by Scanning Electron Microscopy (SEM), to check electrode thickness uniformity and other relevant morphological features.

## 3 Results

Some preliminary tests were performed in order to check the reliability of electrochemical measurements, which have often been reported to be strongly dependent on cell configuration [18, 19, 21, 22]. Cells with different cathode thickness were tested in a symmetrical two- and three-electrode configuration, by alternately using the reference electrode placed at the working or at the counter electrode side. Initial impedance measurements were carried out in

air at open circuit potential. The diagrams showed the expected typical shape independent of cell configuration [16]. The main parameter used to compare cell behaviour was polarisation resistance $R_p$, estimated from the difference between the intercept of frequency dispersion with the real axis at low and high frequency, respectively, in the Nyquist plots. $R_p$ values from the three-electrode and the symmetric two-electrode configurations for a 10 μm thick cathode at different temperatures are plotted in Fig. 1. Half of the $R_p$ values obtained with the symmetrical cell is reported on the y axes. A good agreement in polarisation resistance is obtained in both configurations. Moreover, similar spectra were obtained by placing the reference electrode at both sides of the half cell. The spectra were different only in the intercept with the *x*-axis, due to different electrolyte resistance measured between the working and the reference electrode.

Figure 2 shows the Nyquist plots of the symmetrical cell at different temperatures, at open circuit voltage (OCV), and in air. The plots refer to complete symmetrical cell response; the depressed shape of the spectra suggests a multi-step process.

Impedance diagrams at different oxygen partial pressures and temperatures are plotted in Fig. 3. Spectra are clearly very sensitive to $p(O_2)$ variation, especially in the low frequency region. The plots maintain the typical shape, in which at least two time constants are recognized at each temperature. Impedance data of the symmetric cell were then analysed using a CNLLS-Fit procedure [23], by a

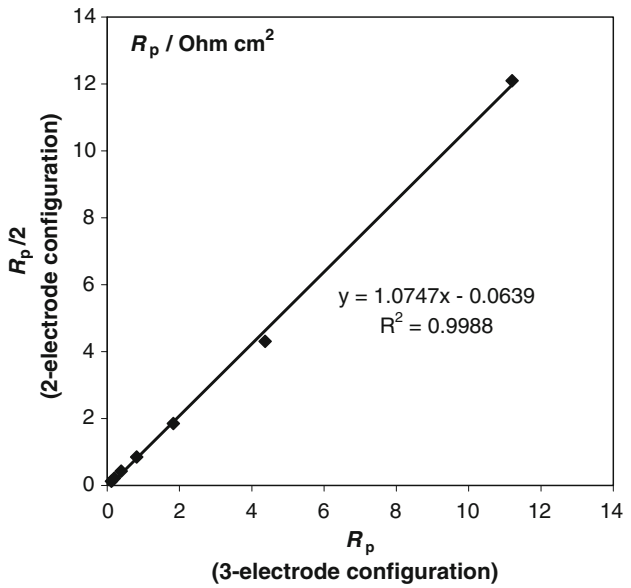


**Fig. 1** Comparison of polarisation resistance $R_p$ extracted from EIS spectra at different temperatures, in a two- and three-electrode configuration. Working conditions: air, open circuit voltage. The values from the symmetric configuration (two-electrode) are reported as half of the $R_p$ extracted from Nyquist plots

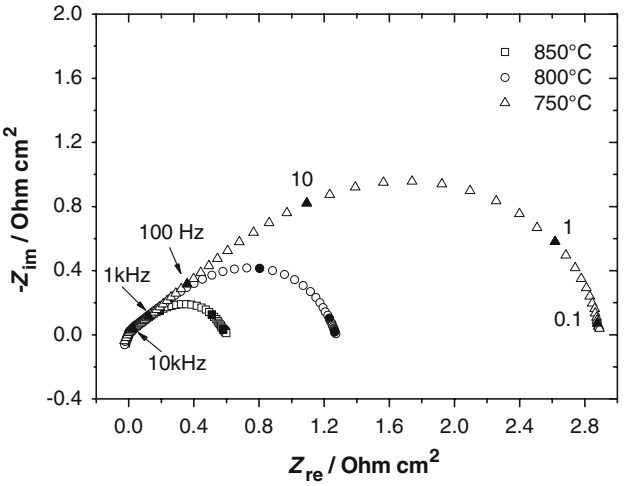


**Fig. 2** Nyquist plots in air at OCV of the symmetric cell with LSM/YSZ composite cathode. About 40 μm cathode thickness

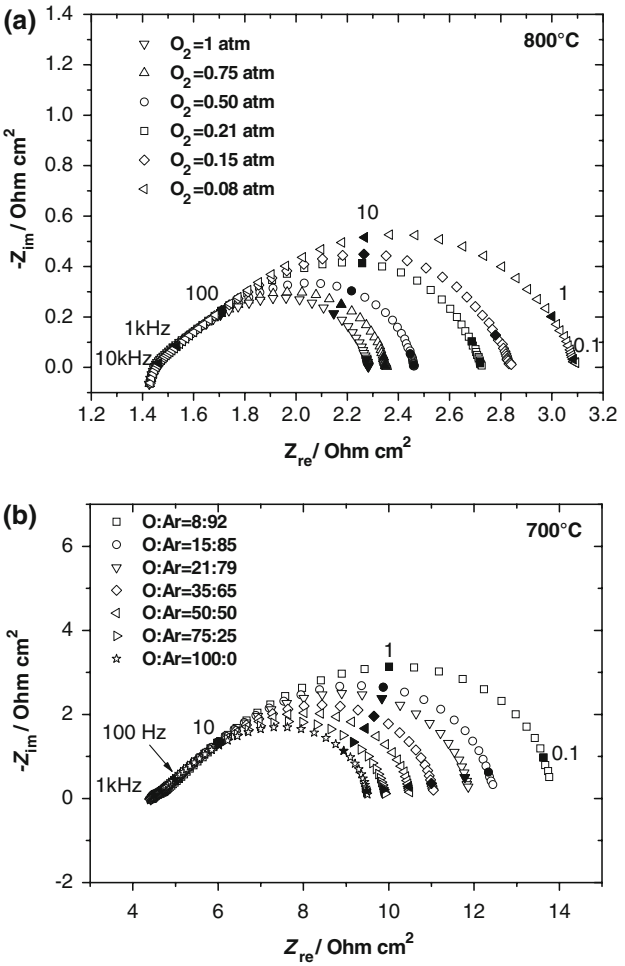


**Fig. 3** Nyquist plots at OCV of the symmetric cell at different oxygen/argon volume ratio: 40 μm cathode thickness

circuit containing two $RZ_Q$ elements, series connected with an $RL$ term: $(R_\Omega L(RZ_Q)_h(RZ_Q)_l)$. $R_\Omega$ is the electrolyte resistance, $L$ is related to cable and cell rig inductance, $(RZ_Q)_h$ and $(RZ_Q)_l$ are referred to the two capacitive loops of the plots at high and low frequency, respectively.

Experimental data extracted at 700 and 800 °C, at $p(O_2) = 0.21$ atm, are compared in Fig. 4 with their fitting. A very good agreement between data and simulation is obtained.

The constant phase element ($Z_Q = Q^{-1}(\mathrm{iw})^{-n}$) was used in the fitting circuit instead of capacitance, since the arcs were slightly depressed. Capacitance and $n$ values were calculated according to an equation given in [24]. At each temperature and for each $p(O_2)$, the parameter $n$ value was very close to 0.5 for the high frequency arc, while it moved towards 0.9 for the low frequency arc. CPE is a very general dispersion element [25]: for $n = 0.5$, it indicates a Warburg behaviour, which suggests ideal semi-infinite diffusion. A value close to 1 suggests capacitive behaviour, which is related to the low frequency arc. This latter element is the main contributor to cathodic resistance. $R_h$ and $R_l$ values obtained with the fitting procedure are plotted versus temperature, at different oxygen partial pressures in Fig. 5. The low frequency resistance follows an Arrhenius behaviour, with 180 kJ mol$^{-1}$ activation energy. Regarding high frequency resistance, a 0.95 correlation factor is obtained with 110 kJ mol$^{-1}$ activation energy.

Impedance measurements at different overvoltages were performed. In Fig. 6, $\ln(1/R_p)$ values are plotted versus overvoltage. As already reported for a smaller set of cells [16], different trends above and below 750 °C can be observed: a linear behaviour of $\log(1/R_p)$ versus $\eta$ at 700 °C is obtained; a deviation from linear behaviour is observed at 750 °C, while, at 800 °C, the trend changes radically and the slope becomes also positive. According to the Butler–Volmer equation, which correlates $\ln(1/R_p)$ to overpotential, such data suggest that oxygen reduction is initially under activation control, while a new regime comes into play for higher temperatures. This is also in agreement with the results of Fig. 5; at low $T$ (right side of Fig. 5), low frequency resistance—which follows an Arrhenius law—is significantly higher than the high frequency one, thus confirming charge transfer control. When the temperature is increased (left side of Fig. 5), low frequency resistance values at different oxygen partial pressures are comparable to those of high frequency resistance. Transport phenomena are no longer negligible. The gaseous diffusion coefficient of molecular oxygen is considerably higher than the diffusivity of oxygen ions in the electrode ionic path. Therefore, it is reasonable to assume that deviation from the linear behaviour of $\ln(1/R_p)$

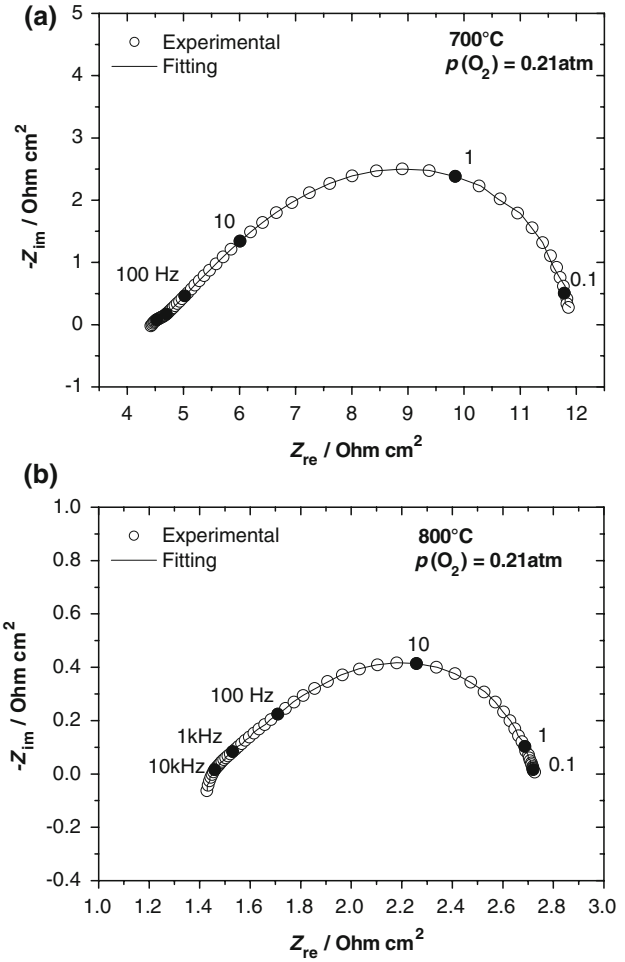


**Fig. 4** Nyquist impedance representation of the symmetric cell at OCV. (○): experimental data; (line): modelling: $(R_\Omega L(RZ_Q)_h(RZ_Q)_l)$. **a** 700 °C: $L = 1.51 \times 10^{-7}$ H; $R_\Omega = 4.454$ Ωcm$^2$; $R_h = 2.26$ Ωcm$^2$; $Q_h = 0.056$; $n_h = 0.472$; $R_l = 5.424$ Ωcm$^2$; $Q_l = 0.027$; $n_l = 0.86$. **b** 800 °C: $L = 3.5 \times 10^{-7}$ H; $R_\Omega = 1.42$ Ωcm$^2$; $R_h = 0.454$ Ωcm$^2$; $Q_h = 0.070$; $n_h = 0.52$; $R_l = 0.859$ Ωcm$^2$; $Q_l = 0.026$; $n_l = 0.88$

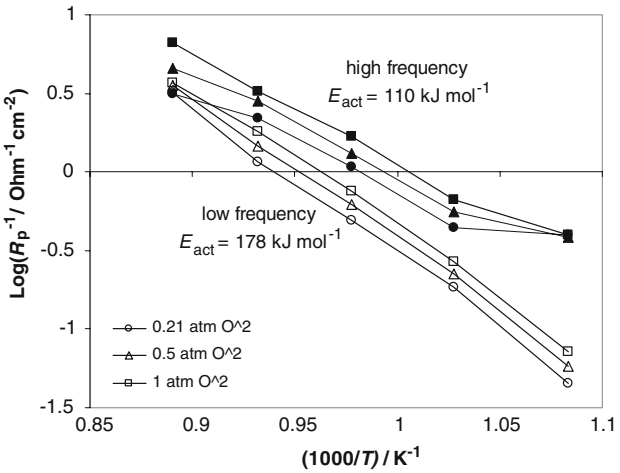


**Fig. 5** Trend of $R_l$ (open symbols) and $R_h$ versus temperature, at different oxygen partial pressures

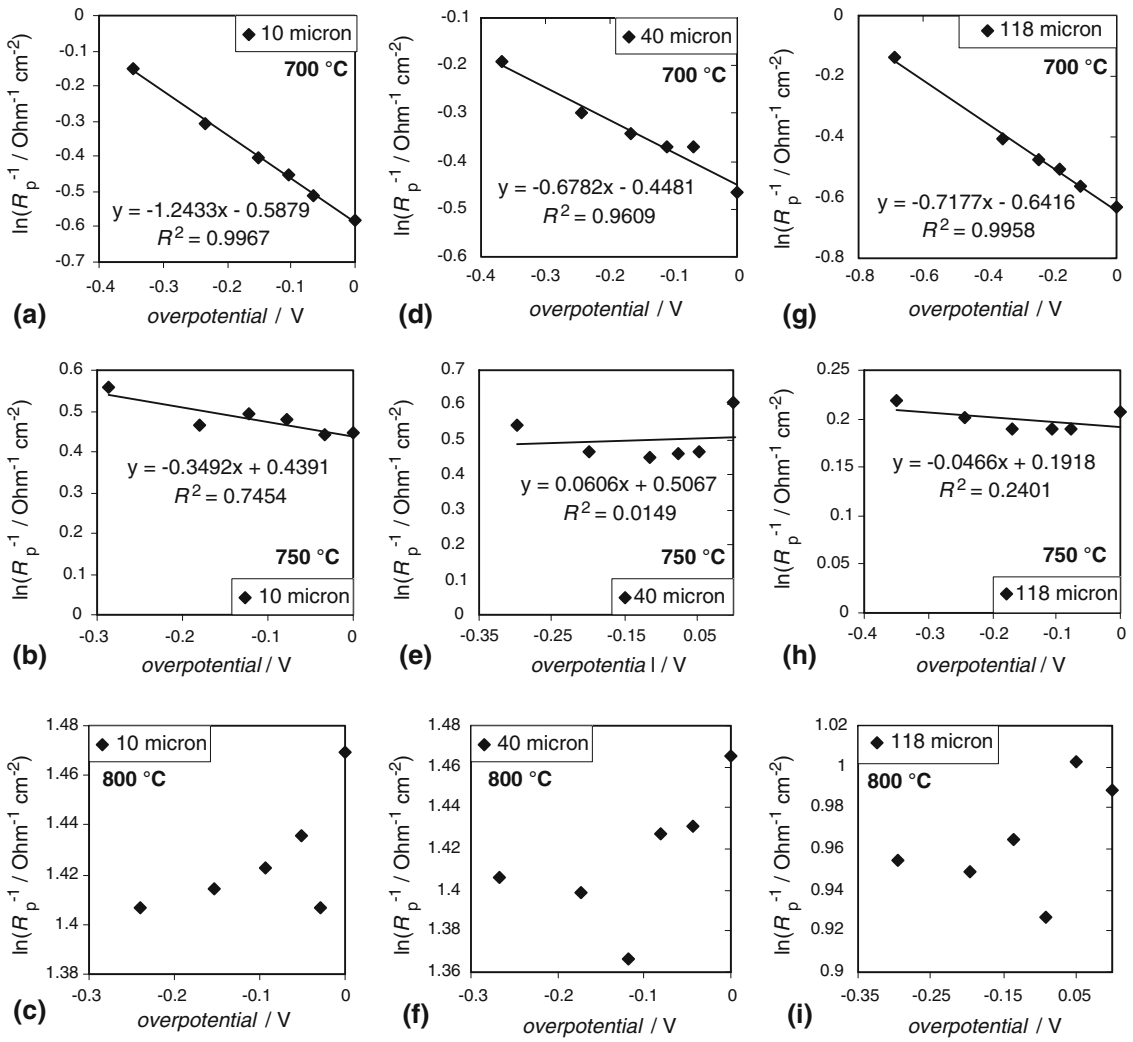


**Fig. 6** Trend of $1/R_p$ versus overpotential. Data extracted from impedance plots at different biases. Left to right: 10, 40, 118 μm thick cathodes

versus $\eta$ is due to ionic transport within the electrode. Ionic transport activation energy of YSZ sintered at 1,100 °C has been calculated by EIS in air at OCV on a two electrode cell: 90 kJ $mol^{-1}$. This is an interesting value, since the YSZ framework within the composite electrode has been sintered under similar conditions. The fact that the $R_h$ trend in the Arrhenius plot of Fig. 5 gives a comparable activation energy shows that ionic transport in the cathode plays a relevant role at high temperature.

The temperature range considered here represents the upper and lower temperature limits for conventional SOFCs and intermediate temperature SOFCs (IT-SOFCs). For both technologies, the materials considered are of practical use. This means that even when made with the same materials, the electrodes should be differently designed depending on their working temperature.

Cathodes with different thicknesses were measured. Relevant $R_p$ values from impedance plots are shown in Fig. 7. These results refer to cells coming from three different batches of cathode slurry with the same composition and prepared according to the same procedure. Electrode morphology, hence performance, strongly depends on parameters such as electrode porosity, distribution, and interconnection of ionic and electronic conductors. These are controlled by the amount of binder in the slurry, the volume ratio between ionic and electronic conductors, as well as ball milling and sintering procedure. Since the samples are small in size, even minor variations in their preparation are significant and are likely to produce scattered data. However, a general decrease in $R_p$ is obtained when electrode thickness increases, with minimum $R_p$ observed for thicknesses in the 25–50 μm range.

Polarisation resistance values for samples with different cathode thickness produced with the same slurry and all sintered at the same time are reported in Fig. 8. From these diagrams, $R_p$ trends depending on the thickness are clearer.

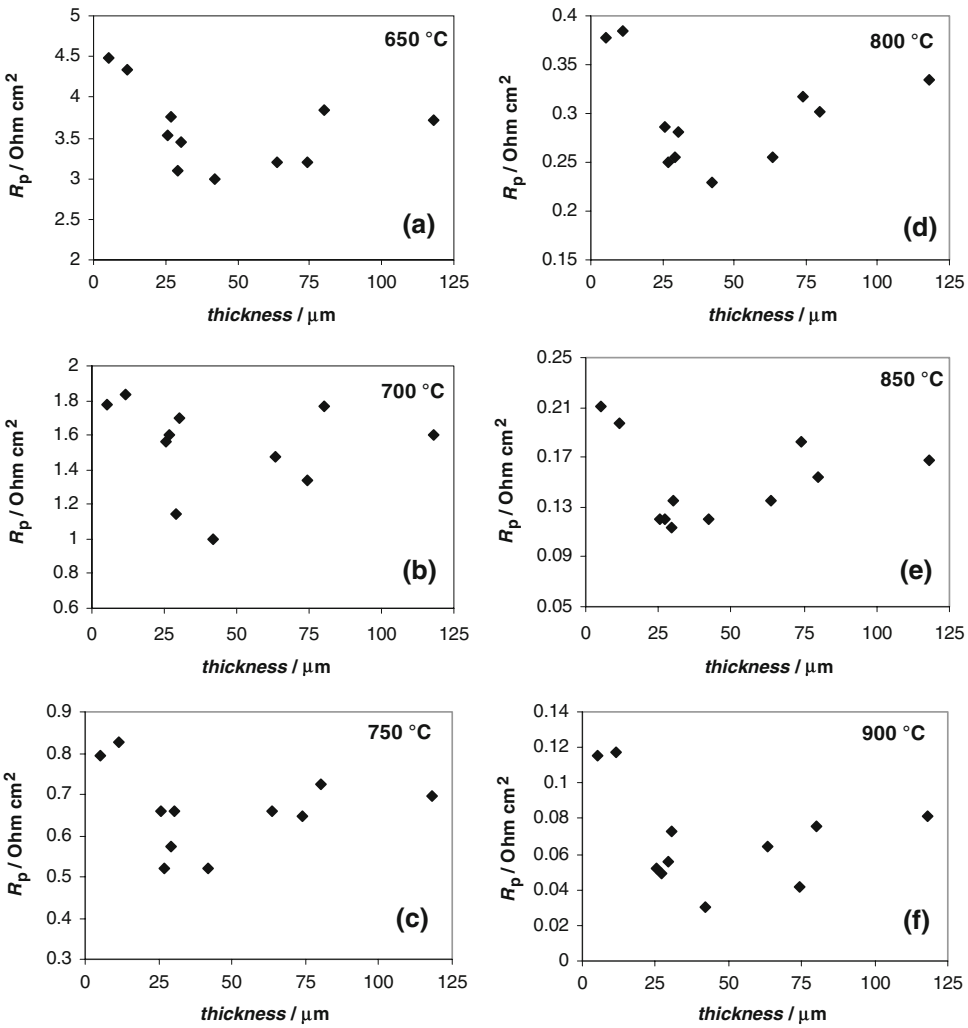


**Fig. 7** Values of polarisation resistances $R_p$ plotted versus thickness, at different temperature values. Cathodes coming from different batches (EIS at OCV in air and in a three-electrode configuration)

The ideal electrode thickness can be observed at around 40 µm, while at lower and higher electrode thickness a higher resistance is recorded. Also Virkar et al. [26] found a decrease or an increase in charge transfer resistance with increasing cathode thickness, depending on ionic conductivity. However, they found an asymptotic value with thicker electrodes, which we did not find in our work. Kenjo and Nishiya [27] and Juhl et al. [28] found a decrease in polarisation resistance with thickness, but they analysed composite cathodes up to 20 µm.

Since these results have been obtained under open circuit potential and the current load on the electrode might change the impact of the phenomena, polarisation measurements have also been performed.

In all polarisations (Fig. 9), there is a sharp current decrease, whenever electrode thickness is raised from 16 to 32 µm. A further, although less important, kinetic improvement is achieved with the 40 µm thick electrode; conversely, the curve of the 60 µm thick electrode decreases, overlapping or falling even below the curve of the 32 µm electrode. A remarkable decrease in current is recorded with the thickest electrode.

Owing to these results, cathode microstructure has been considered to be a key factor in understanding the system under investigation. Thus, after electrochemical measurements, the cells were cut and observed by SEM. Some defects were detected inside the electrode bulk. However, after a quantitative evaluation, it was estimated that they affect a very low fraction of total electrode volume with no interruption of current paths across the electrode thickness.

Variations in key morphological properties (e.g. porosity) together with composite cathode thickness were assessed by SEM. Some images of three cathodes with 10, 30, and 70 µm thicknesses are presented in Fig. 10. Two samples for each thickness are considered in this figure. In each photograph, cathode layers of different thicknesses that have built up on the dense electrolyte can be readily identified (on the left hand side of each photograph). Each cathode image is processed by image

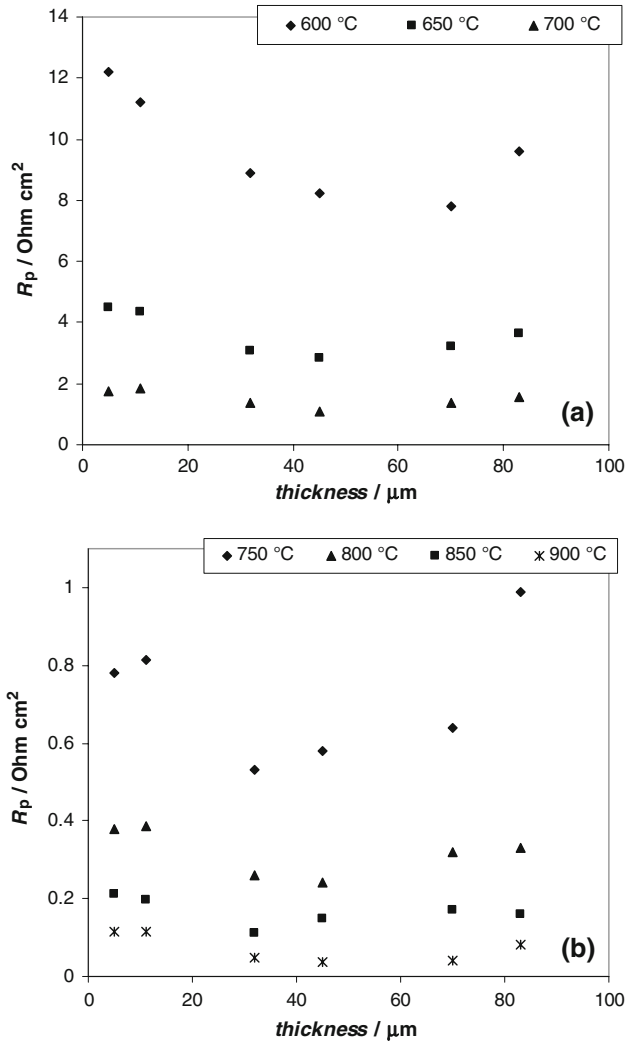


**Fig. 8** Values of polarisation resistances $R_p$ plotted versus thickness, at different temperatures. Cathodes coming from the same batch. (EIS at OCV in air and in a three-electrode configuration)

analysis to estimate grey level variations along the axial coordinate. For this reason, cathode thickness was divided into 5 µm sub-layers. The grey level was determined by image analysis in each sub-layer of every sample. The results are shown in Fig. 11, which shows grey level variations in each sample determined at varying distance from the cathode free surface (opposite to the cathode-electrolyte interface). The relative grey level in Fig. 11 is calculated as:

$$\gamma = \frac{g}{g_{\max}}$$

where $g$ is the grey level determined by image analysis of the different cathode layers in SEM pictures and $g_{\max}$ is the maximum grey level determined at the free surface of the cathodes (opposite to the electrolyte side).

As can be observed in Fig. 11, the grey level gradient is similar in all layers placed at the same distance from the cathode free surface. As a consequence, the relative grey level in all cathodes can be computed using the same linear relationship with the distance from the free surface, obtained as the best linear fitting of data in Fig. 11.

These results confirm that cathode morphological properties vary along its axial coordinate. It is reasonable to assume that the solid volume fraction in any cathode layer is proportional to the grey level, i.e. the solid volume fraction linearly decreases along the axial coordinate with the same slope as the best linear fitting of the data presented in Fig. 11.

This analysis shows that electrode porosity at the electrolyte/electrode interface increases with increasing electrode thickness. From a qualitative point of view, it seems that two effects may play a relevant role. The first is that the increase in electrode thickness increases the number of active sites, thus leading to enhanced electrodes with low $R_p$. On the other hand, higher porosity at the electrolyte/electrode interface in thick electrodes leads to a local increase in ionic path resistivity. This latter fact is not negligible, especially because, in composite cathodes, ionic current makes up the bulk of total current flowing close to this interface. In this situation an optimal electrode thickness could be identified, justifying the electrochemical results obtained.

## 4 Conclusions

The measurements performed with different cell configurations help improve the reliability of electrochemical results. The electrodes have been produce with a procedure widely applied in SOFC studies. The analysis performed allowed focus on: (i) the phenomena playing relevant roles in oxygen reduction, (ii) the importance of geometry and microstructure in electrode performance optimisation.

Impedance diagrams show two time constants. The fitting procedure, performed with the simple equivalent circuit presented here, gives good results. Considering the electrochemical results under polarisation in the cell with a three electrode configuration charge transfer is the rate determining step at low temperatures. A second process, which prevails at higher temperature, is due to ionic transport within the electrode. Furthermore, the interplay between these two main phenomena in the overall process has been highlighted. The possibility to change cell configuration, as well as modulate parameters like temperature, reagent partial pressure and polarisation, is very useful to understand the system. Moreover, the use of simple models like CNLLS contributes to the final results.

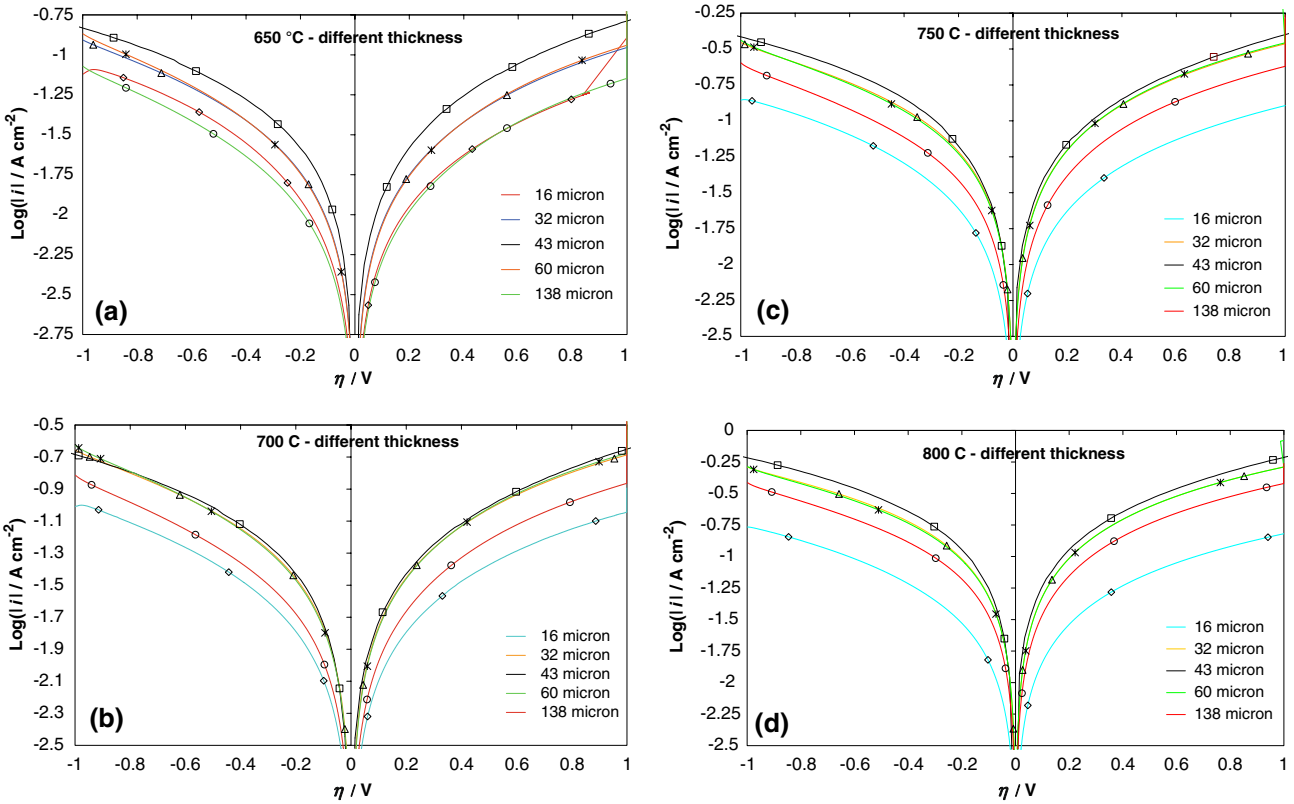


**Fig. 9** Polarisation curves in air of composite cathodes with different thickness: ◇ 16, × 32, □ 43, △ 60, ○ 138 μm

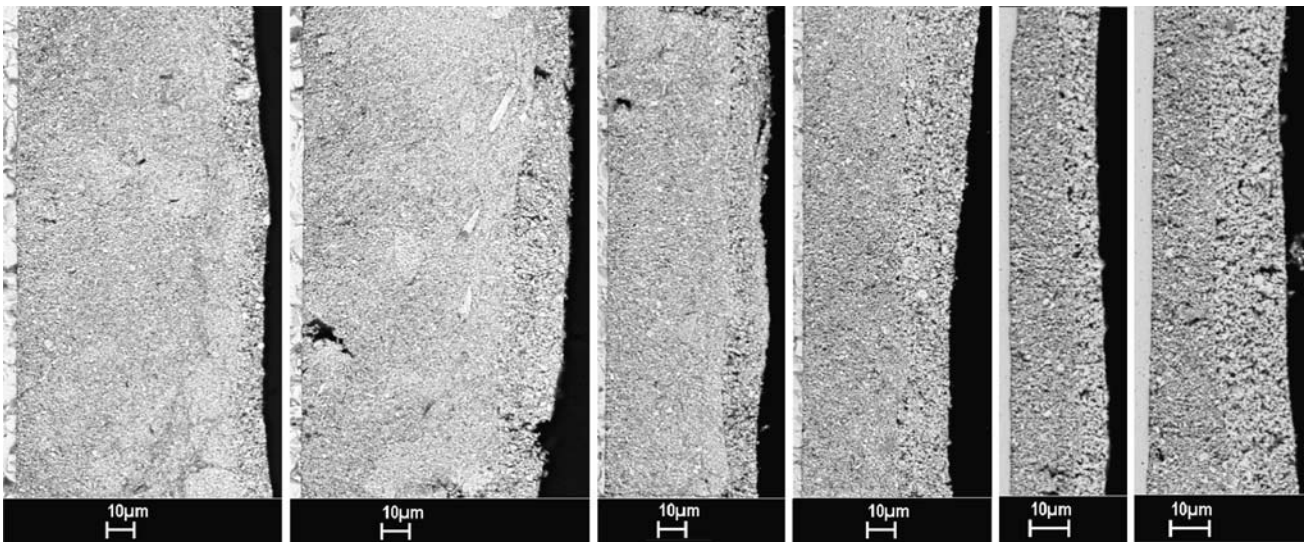


**Fig. 10** SEM pictures of porous composite cathode with different thickness

The measurements performed at OCV and under polarisation at different temperatures show that an optimal electrode thickness exists, which is strongly related to its microstructure. These data underline that geometry-microstructure of the electrode and operating conditions play a significant role in electrode performance optimisation. Finally, this paper supplies additional results to recently published data [16], thus allowing for advanced theoretical analysis of the overall process in which system morphological properties (porosity i.e. number of contact points and tortuosity of the ionic-electronic paths) may be included.

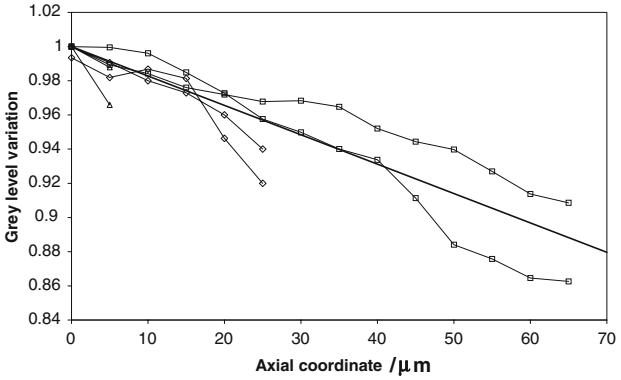


**Fig. 11** Axial gradient of grey level in porous composite cathodes with different thickness

**Acknowledgements** The authors gratefully acknowledge the financial support of the Italian project "FISR: Nanosistemi Inorganici ed Ibridi per lo Sviluppo e l'Innovazione di Celle a Combustibile".

## References

1. Tao S, Irvine JTS, Kilner JA (2005) Adv Mater 17:1734–1737
2. Peña-Martínez J, Marrero-López D, Pérez-Coll D, Ruiz-Morales JC, Núñez P (2007) Electrochim Acta 52:2950–2958
3. Shao Z, Haile SM (2004) Nature 431:170–173
4. Lv H, Tu H-y, Zhao B-y, Wu Y-j, Hu K-a (2007) Solid State Ionics 177:3467–3472
5. Tao S, Irvine JTS (2003) Nat Mater 2:320–323
6. Goodenough JB, Huang Y-H (2007) J Power Sources 173:1–10
7. Jung HY, Kim W-S, Choi S-H, Kim H-C, Kim J, Lee H-W, Lee J-H (2006) J Power Sources 155:145–151
8. Piccardo P, Chevalier S, Molins R, Viviani M, Caboche G, Barbucci A, Sennour M, Amendola R (2006) Surf Coat Technol 201(7):4471–4475
9. Ucida H, Arisaka S, Watanabe M (2000) Solid State Ionics 135:347–351
10. Liu M, Dong D, Peng R, Gao J, Diwu J, Liu X, Meng G (2008) J Power Sources 180:215–220
11. Schneider LCR, Martin CL, Bultel Y, Dessemond L, Bouvard D (2007) Electrochim Acta 52:3190–3198
12. Kim J-S, Pyun S-I, Shin H-C, Kang S-JL (2008) J Electrochem Soc 155(7):B762–B769
13. Hammouche A, Schouler EJL, Henault M (1988) Solid State Ionics 28–30:1205–1207
14. Mizusaki J, Tagawa H, Naraya K, Sasamoto T (1991) Solid State Ionics 49:111–118
15. Takeda Y, Sakaki Y, Ichikawa T, Imanishi N, Yamamoto O, Mori M, Mori N, Abe T (1994) Solid State Ionics 72(2):257–264
16. Barbucci A, Carpanese MP, Reverberi AP, Cerisola G, Blanes M, Cabot PL, Viviani M, Bertei A, Nicolella C (2008) J Appl Electrochem 38:939–945
17. Nicolella C, Bertei A, Barbucci A, Vatistas N (2008) J Appl Electrochem. doi:10.1007/s10800-008-9691-3
18. Winkler J, Hendriksen PV, Bonanos N, Mogensen M (1998) J Electrochem Soc 145(4):1184–1192
19. Adler SB (2002) J Electrochem Soc 149(5):E166–E172
20. Macdonald JR (1987) Impedance spectroscopy. Wiley, New York
21. Hsieh G, Mason TO, Garboczi EJ, Pederson LR (1997) Solid State Ionics 96:153–172
22. Rutman J, Riess I (2008) Placement of reference electrode in solid state electrolyte cells. Solid State Ionics. doi:10.1016/j.ssi.2008.01.071(in press)
23. Boukamp BA (1986) Solid State Ionics 20:31–44
24. Fleig J (2002) Solid State Ionics 150:181–193
25. Stoynov Z, Vladikova D (2005) Differential impedance analysis. Marin Drinov Academic Publishing House, Sofia
26. Virkar AV, Chen J, Tanner CW, Kim J-W (2000) Solid State Ionics 131:189–198
27. Kenjo T, Nishiya M (1992) Solid State Ionics 57:295–302
28. Juhl M, Primdahl S, Manon C, Mogensen M (1996) J Power Sources 61:173–181